

Growth of PbTe nanowires by molecular beam epitaxy

Citation for published version (APA):

Schellingherhout, S. G., De Jong, E. J., Gomanko, M., Guan, X., Jiang, Y., Hoskam, M. S. M., Jung, J., Koelling, S., Moutanabbir, O., Verheijen, M. A., Frolov, S. M., & Bakkers, E. P. A. M. (2022). Growth of PbTe nanowires by molecular beam epitaxy. *Materials for Quantum Technology*, 2(1), Article 015001.
<https://doi.org/10.1088/2633-4356/ac4fba>

Document license:

CC BY

DOI:

[10.1088/2633-4356/ac4fba](https://doi.org/10.1088/2633-4356/ac4fba)

Document status and date:

Published: 01/03/2022

Document Version:

Publisher's PDF, also known as Version of Record (includes final page, issue and volume numbers)

Please check the document version of this publication:

- A submitted manuscript is the version of the article upon submission and before peer-review. There can be important differences between the submitted version and the official published version of record. People interested in the research are advised to contact the author for the final version of the publication, or visit the DOI to the publisher's website.
- The final author version and the galley proof are versions of the publication after peer review.
- The final published version features the final layout of the paper including the volume, issue and page numbers.

[Link to publication](#)

General rights

Copyright and moral rights for the publications made accessible in the public portal are retained by the authors and/or other copyright owners and it is a condition of accessing publications that users recognise and abide by the legal requirements associated with these rights.

- Users may download and print one copy of any publication from the public portal for the purpose of private study or research.
- You may not further distribute the material or use it for any profit-making activity or commercial gain
- You may freely distribute the URL identifying the publication in the public portal.

If the publication is distributed under the terms of Article 25fa of the Dutch Copyright Act, indicated by the "Taverne" license above, please follow below link for the End User Agreement:

www.tue.nl/taverne

Take down policy

If you believe that this document breaches copyright please contact us at:

openaccess@tue.nl

providing details and we will investigate your claim.

PAPER • OPEN ACCESS

Growth of PbTe nanowires by molecular beam epitaxy

To cite this article: Sander G Schellingerhout *et al* 2022 *Mater. Quantum. Technol.* **2** 015001

View the [article online](#) for updates and enhancements.

You may also like

- [Structural and dielectric properties of prepared PbS and PbTe nanomaterials](#)
A. A. Azab, Azza A. Ward, G. M. Mahmoud et al.
- [Strategies for optimizing the thermoelectricity of PbTe alloys](#)
Jinze Zhai, Teng Wang et al.
- [Electrochemical epitaxial PbTe nanowires photodetector for NIR response](#)
Zhongmin Guo, Zhisheng Zhang, Ruiyang Yan et al.

Materials for Quantum Technology



PAPER

Growth of PbTe nanowires by molecular beam epitaxy

OPEN ACCESS

RECEIVED
20 October 2021

REVISED
17 January 2022

ACCEPTED FOR PUBLICATION
27 January 2022

PUBLISHED
22 February 2022

Original content from this work may be used under the terms of the [Creative Commons Attribution 4.0 licence](#).

Any further distribution of this work must maintain attribution to the author(s) and the title of the work, journal citation and DOI.



Sander G Schellingerhout¹ , Eline J de Jong¹, Maksim Gomanko², Xin Guan¹ , Yifan Jiang² , Max S M Hoskam¹ , Jason Jung¹ , Sebastian Koelling³ , Oussama Moutanabbir³ , Marcel A Verheijen¹ , Sergey M Frolov² and Erik P A M Bakkers^{1,*}

¹ Department of Applied Physics, Eindhoven University of Technology, 5600MB, Eindhoven, The Netherlands

² Department of Physics and Astronomy, University of Pittsburgh, Pittsburgh, Pennsylvania 15260, United States of America

³ Department of Engineering Physics, École Polytechnique de Montréal, C.P. 6079, Succ. Centre-Ville, Montréal, Québec, H3C 3A7, Canada

* Author to whom any correspondence should be addressed.

E-mail: e.p.a.m.bakkers@tue.nl

Keywords: PbTe, nanowires, MBE

Supplementary material for this article is available [online](#)

Abstract

Advances in quantum technology may come from the discovery of new materials systems that improve the performance or allow for new functionality in electronic devices. Lead telluride (PbTe) is a member of the group IV–VI materials family that has significant untapped potential for exploration. Due to its high electron mobility, strong spin–orbit coupling and ultrahigh dielectric constant it can host few-electron quantum dots and ballistic quantum wires with opportunities for control of electron spins and other quantum degrees of freedom. Here, we report the fabrication of PbTe nanowires by molecular beam epitaxy. We achieve defect-free single crystalline PbTe with large aspect ratios up to 50 suitable for quantum devices. Furthermore, by fabricating a single nanowire field effect transistor, we attain bipolar transport, extract the bandgap and observe Fabry–Pérot oscillations of conductance, a signature of quasiballistic transmission.

1. Introduction

Semiconductor nanowires (NWs) are a widely studied platform for quantum transport devices [1] due to the quasi-1D confinement that stems from the small radius (<100 nm) and high aspect ratio. By combining a semiconductor NW with a superconductor, a topological superconductor can be realized in which Majorana zero modes are expected [2–5]. By defining quantum dots, e.g. using gate potentials, spin qubits can be studied, while in NW Josephson junctions gate-tunable transmon qubits were realized [6]. A substantial fraction of the research in the field of NW quantum computation is focused on III–V semiconductors, such as InSb and InAs [2–5]. Group IV nanowires, such as Ge/Si core–shell wires, were recently used to demonstrate ultrafast spin qubit control [7].

At the same time, group IV–VI materials have been extensively studied in the 2D geometry [8], but are relatively unexplored as NWs, despite their potential and attractive characteristics for quantum transport experiments [9, 10]. Here, we focus on lead telluride (PbTe) NWs which as we show form single crystal, defect free NWs. PbTe has large *g*-factors, a high bulk carrier mobility [11] of over 10^6 cm² Vs⁻¹ and strong spin–orbit coupling. Most importantly, PbTe has an extremely high static dielectric constant of 1400 at 4.2 K [12], which is about two orders of magnitude higher than that of group III–V or IV semiconductors. Owing to this high dielectric constant, charged defects are effectively screened and contribute less to disorder. In addition, PbTe could be combined with Pb, which has one of the highest critical temperature of the elemental superconductors. Potentially, a pristine PbTe–Pb interface can be created without inducing interface reactions.

The key finding of this paper is that molecular beam epitaxy (MBE) is a powerful method for synthesizing high aspect ratio defect free PbTe NWs. Previously, PbTe NWs have been synthesized by using electrochemical

deposition resulting in polycrystalline growth [13, 14], by using a hydrothermal process [15] and by chemical vapor techniques resulting in electron mobilities around $1 \text{ cm}^2 \text{ Vs}^{-1}$ [16–19].

In MBE, in contrast, growth takes place in an ultra-pure environment and can be controlled at a sub-monolayer level. Growth of single-crystalline PbTe NWs in MBE has been reported [20, 21]. Dziawa *et al* [20] have grown PbTe wires by the vapor–liquid–solid (VLS) growth mode using self-organized Au droplets on a GaAs(111)B substrate. Most important challenges to study and exploit the electronic properties of the reported PbTe NWs are (1) their limited length making it difficult to accommodate multiple electrodes which is necessary for device fabrication and measurement; (2) the tapering of the wires leading to a non-flat surface and a non-uniform quantization energy along the NW length. Volobuev *et al* [21] have grown PbTe NWs from Bi-catalysts, preventing tapering at the cost of unintentionally doping the NWs with Bi.

In this work, we address the two main challenges of this material system. We investigate the PbTe NWs growth dynamics in MBE and by tuning the growth parameters, we obtain long, untapered wires with a large aspect ratio. The wires are single crystalline, do not contain foreign impurities above the few ppm level, and from low temperature transport experiments we find that electron transport between the contacts is either ballistic or quasiballistic. Thus, our PbTe NWs show features not previously shown in NWs of this material system, and offer a promising platform for more advanced quantum transport experiments and device fabrication.

2. Experimental

Au-catalysed PbTe NWs are grown on GaAs(111)B substrates. Details on substrate fabrication can be found in supporting information section 1 (<https://stacks.iop.org/MQT/2/015001/mmedia>). The GaAs substrate is indium soldered on a sample holder and degassed in high vacuum at $300 \text{ }^\circ\text{C}$ for 60 min before being introduced to the MBE growth chamber. We use elemental Pb and Te cells to precisely control the Pb/Te fluxes. The individual beam equivalent pressure of each cell is measured using a naked Bayard–Alpert gauge which can be moved in front of the sample holder. The growth time is 3 h and 40 min unless noted otherwise. The growth temperature is measured using a commercial kSA BandiT system. Additional growth information can be found in supporting information section 2.

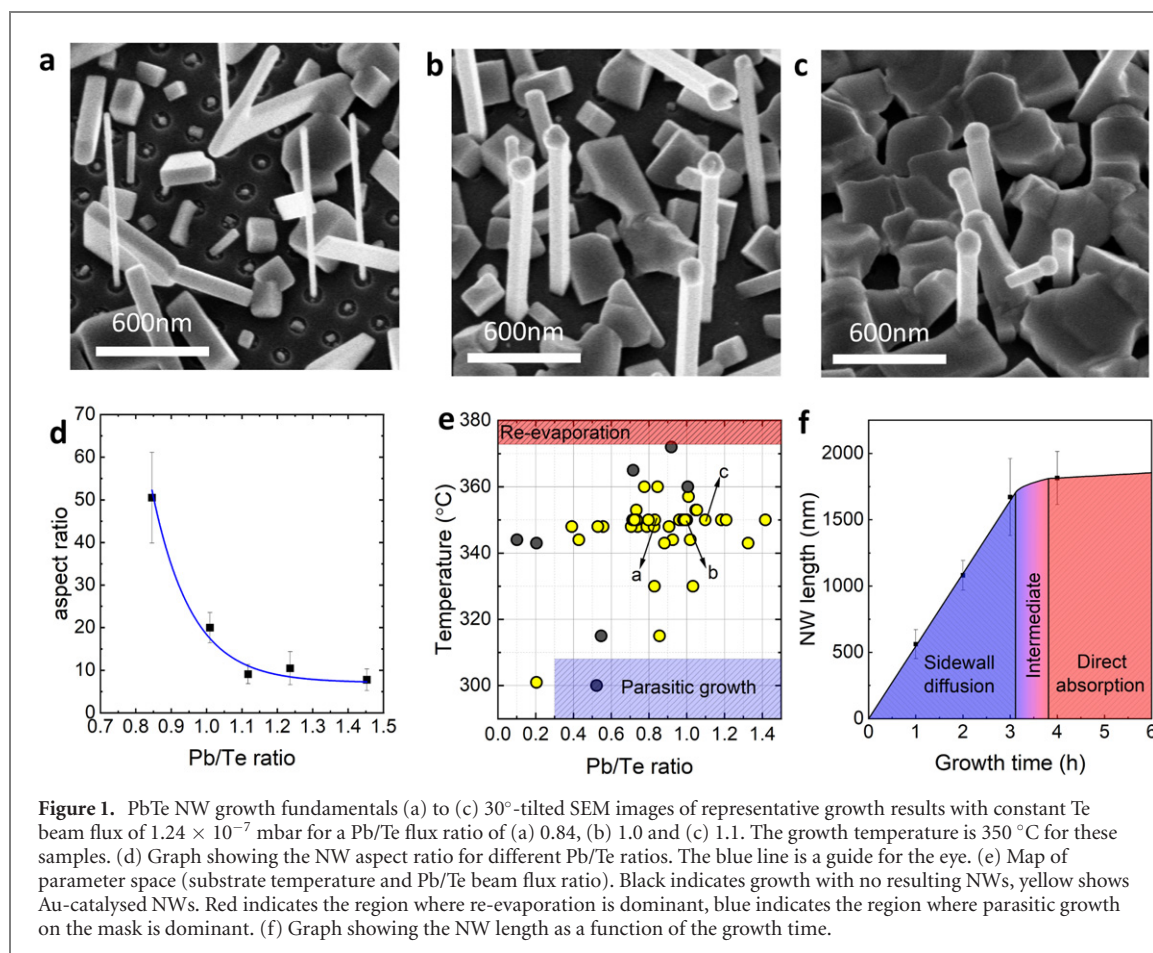
Transmission electron microscopy (TEM) studies were performed using a probe-corrected JEOL ARM 200F, operated at 200 kV. The TEM is equipped with a 100 mm^2 SDD Centurio energy dispersive x-ray spectroscopy (EDX) detector. The nanowires have been transferred to a holey carbon film by swiping the holey carbon film over the substrate containing the NWs.

Samples for atom probe tomography (APT) were prepared by transferring NWs in a FEI Helios Nanolab 660 DualBeam system using a method described in detail by Koelling *et al* [22]. APT was carried out on a LEAP 4000X-HR from Cameca with a laser producing picosecond pulses at 355 nm at a repetition rate of a 65 kHz. For the analyses laser pulse energies between 5 and 10 pJ were used and a voltage of 2.5–3 kV was applied. The machine has a single ion detection system with an efficiency of $\sim 35\%$. The APT data were reconstructed with IVAS 3.8.5a34. Due to the relatively low voltage applied during the measurement [23], a comparatively high ratio of $\sim 25\%$ multi-hit events [24] and the heavy elements analyzed in this work the detection system does not fully perform up to specifications and the lighter Pb ions, that typically arrive at the detector first during a multi-hit event, make up $\sim 60\%$ of the measured bulk concentration of the stoichiometric PbTe.

Single NW field effect transistor (FET) devices are fabricated on highly p-doped Si(100) substrates that act as a global back gate, provided with a 285 nm thermal SiO₂ layer on top. NWs are transferred from the growth substrate to the device substrate by mechanical transfer and are located using a scanning electron microscope (SEM). To write the contacts, a double layer of PMMA (495 A4 and 950 A2) is spun at 5000 RPM for 60 s and baked for 15 min at $175 \text{ }^\circ\text{C}$. Using the SEM images as reference the design is written using EBL. The resist is developed in MIBK:IPA (ratio 1:3) for 60 s, and rinsed in IPA for 60 s. A descum is done using a short (15 s at 50 W) oxygen plasma exposure to remove any remaining resist from the exposed areas. The NW native oxide is removed by applying argon milling, after which a Ti/Au (10 nm/140 nm) layer is deposited *in situ* via electron beam evaporation. The remaining polymer is removed in acetone, which subsequently lifts off the Ti/Au from unexposed areas. An additional top gate is deposited, as this allows stronger coupling to the NW. Using atomic layer deposition at $120 \text{ }^\circ\text{C}$ a 10 nm HfO₂ dielectric layer is deposited. For the fabrication of top gates, a similar recipe is used. The same PMMA double layer is used with subsequent EBL, development and oxygen descum. A Ti/Au (10/130 nm) layer is deposited and lift-off is done overnight in acetone, followed by a rinse in IPA.

3. Results and discussion

We start by investigating the PbTe NW growth dynamics with the aim to obtain high aspect ratio single crystalline NWs using the VLS mechanism. The main experimental parameters are the substrate temperature and



the Pb/Te flux ratio. Figures 1(a)–(c) show scanning electron microscopy (SEM) images of PbTe NWs grown at 350 °C for varying Pb/Te flux ratios. We find PbTe NWs as well as more isotropically grown, faceted crystalline objects. The NW aspect ratio depends on the Pb/Te flux ratio. In case $\text{Pb/Te} < 1$ (figure 1(a)), long and thin NWs are grown with a small catalyst droplet on the top. The NWs have grown from the patterned catalysts confirming the VLS growth mechanism, and have a length ranging from 2 to 3 μm , with a diameter of 40 ± 10 nm. A large proportion of the NWs grow perpendicular or near perpendicular to the surface, the long axis being the [100] axis, as will be discussed below. Based on the orientations of the side facets, we can conclude there is no fixed crystallographic orientation orthogonal to the long axis, indicating that the NWs do not have an epitaxial relationship to the substrate. Increasing the Pb flux to $\text{Pb/Te} = 1$ (figure 1(b)) leads to NWs with a larger catalyst droplet due to the increased incorporation of Pb in the Au catalyst and in turn a larger NW diameter of 85 ± 15 nm and a decreased length of 1.4 to 1.8 μm . In figures 1(a) and (b), most of the NWs and faceted crystals are grown from the patterned holes, showing strong growth selectivity gained by the applied SiN_x mask, although parasitic growth on the mask is not fully suppressed. At $\text{Pb/Te} > 1$ (figure 1(c)) the excess Pb leads to NWs with a reduced aspect ratio, a diameter of 105 ± 15 nm and a length of 0.8 to 1.0 μm , as well as a large amount of parasitic growth. We do not observe tapering in any of the as-grown PbTe NWs. The random orientations of the crystals emerging from the holes are attributed to the native oxide on the GaAs substrate, preventing an epitaxial relation between the PbTe and the underlying substrate. We have found no regime where only NWs are grown. Despite significant efforts, we have not found a regime with a higher yield of NWs ($< 4\%$) than illustrated in figures 1(a)–(c). Despite the low yield we believe that the observed trends are representative for the study. Figure 1(d) summarizes the aspect ratio as a function of the Pb/Te flux ratio, showing a dramatic increase in aspect ratio for decreasing Pb/Te flux ratios. The catalyst droplet size increases with the Pb/Te flux ratio leading to thicker wires. A stable, but smaller aspect ratio is found for $\text{Pb/Te} > 1$, where the catalyst droplet is gradually saturated with Pb and reaches its maximum size. The excess Pb stimulates uncontrolled crystal growth on the substrate surface.

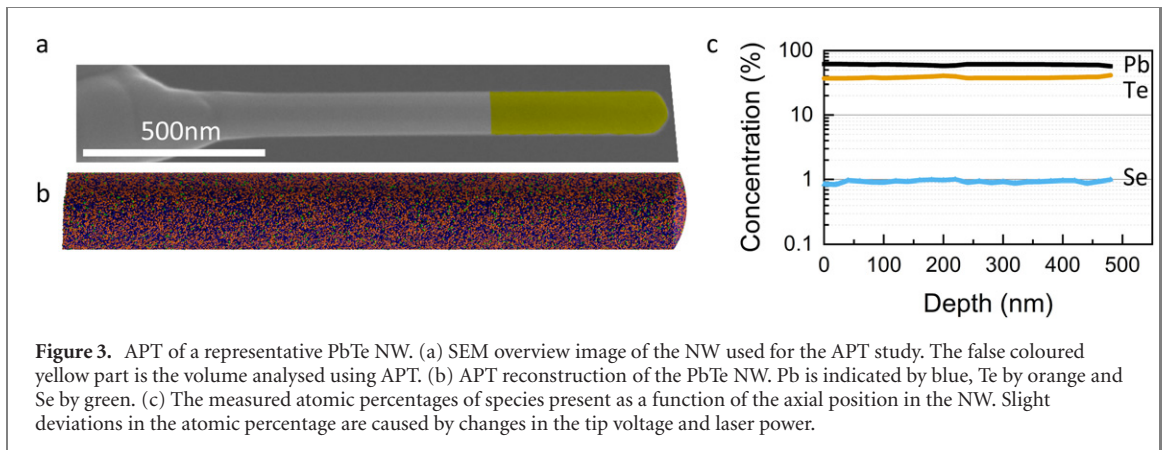
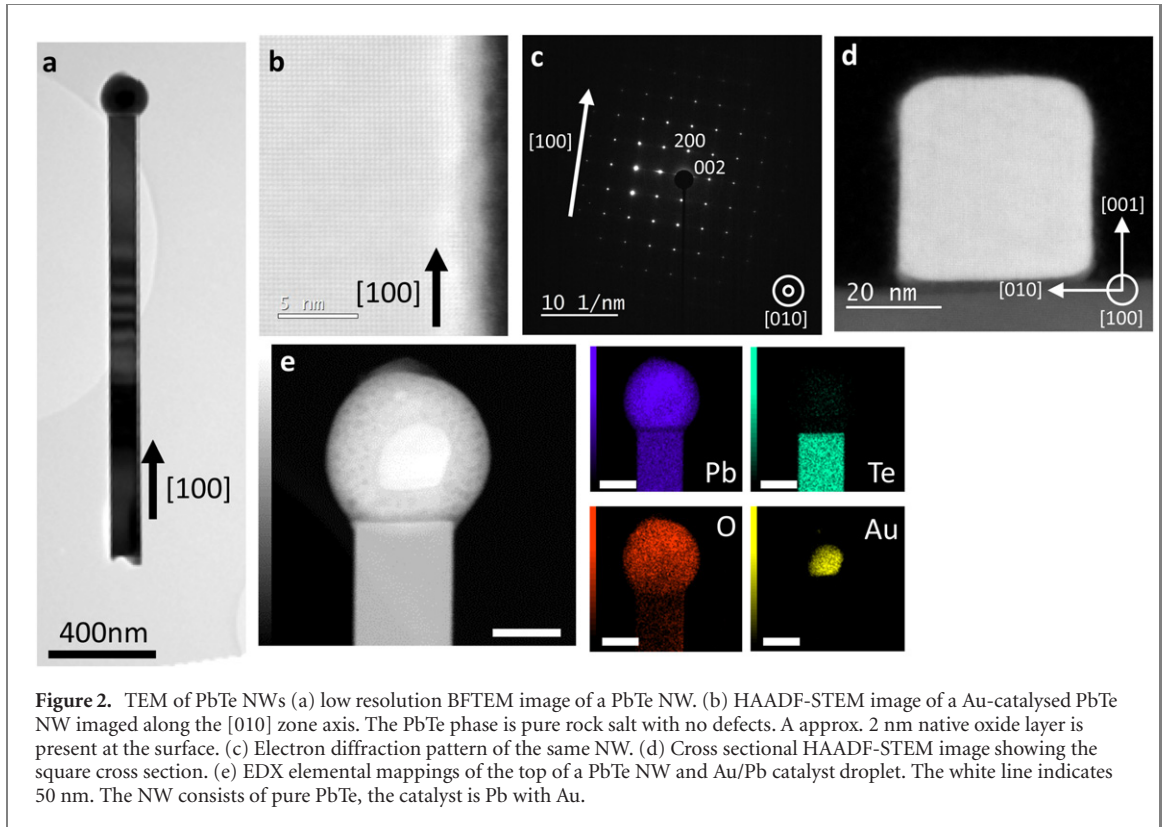
As both Pb and Te have a high vapor pressure it is important to note that the growth temperature strongly affects the quantity of effective adatoms on the sample surface via re-evaporation, which means the total supplied flux and the Pb/Te flux ratio has to be adjusted based on the temperature. The parameter window,

substrate temperature versus Pb/Te ratio, for PbTe NW growth is summarized in figure 1(e). The growth conditions that result in Au-catalysed NWs (arbitrarily defined here by an aspect ratio larger than 5) are highlighted in yellow, with black indicating conditions not leading to NW growth. PbTe NW growth has been observed with a substrate temperature between 270 and 360 °C and Pb/Te ratios from 0.2 to 1.4. The optimum growth temperature is identified at $T_{\text{opt}} = 355 \pm 5$ °C at a Pb/Te ratio slightly below 1. It is important to note that at higher Pb/Te flux ratios parasitic growth becomes much more pronounced due to the excess of Pb. For a low Pb/Te flux ratio (0.2), PbTe NW growth is observed at temperatures down to 270 °C. In the blue shaded area (Pb/Te > 0.3, $T < 310$ °C) parasitic growth dominates over NW growth. Above 370 °C (shaded red) the adatom re-evaporation rate becomes too high and the PbTe is unstable, preventing NW growth. The Pb/Te flux ratio tunability facilitates the study of the electronic properties of the PbTe NWs, as the free carrier type (n- or p-type) can be tuned by this ratio resulting in Pb or Te vacancies [25]. It is important to note that although the three different Pb/Te flux ratio regimes presented in figures 1(a)–(c) result in different NW morphologies, all three yield single-crystalline NWs, as presented in SI figure 2. Finally, the NW growth rate is investigated for the optimum Pb/Te ratio of 0.9 and a growth temperature of 360 °C (figure 1(f)). The NW length increases linearly with time until a length of approximately 1.8 μm . When growth time exceeds 3 h, the growth rate strongly decreases, indicating that the main driving mechanism of the growth is adatom diffusion over NW sidewalls instead of direct absorption of species into the catalyst droplet. The total NW length is thus limited by the adatoms, which can no longer reach the catalyst droplet before being re-evaporated. We observe longer NWs for a lower Pb/Te flux ratio, which indicates an increased sidewall diffusion length due to the increased Te presence around the NW.

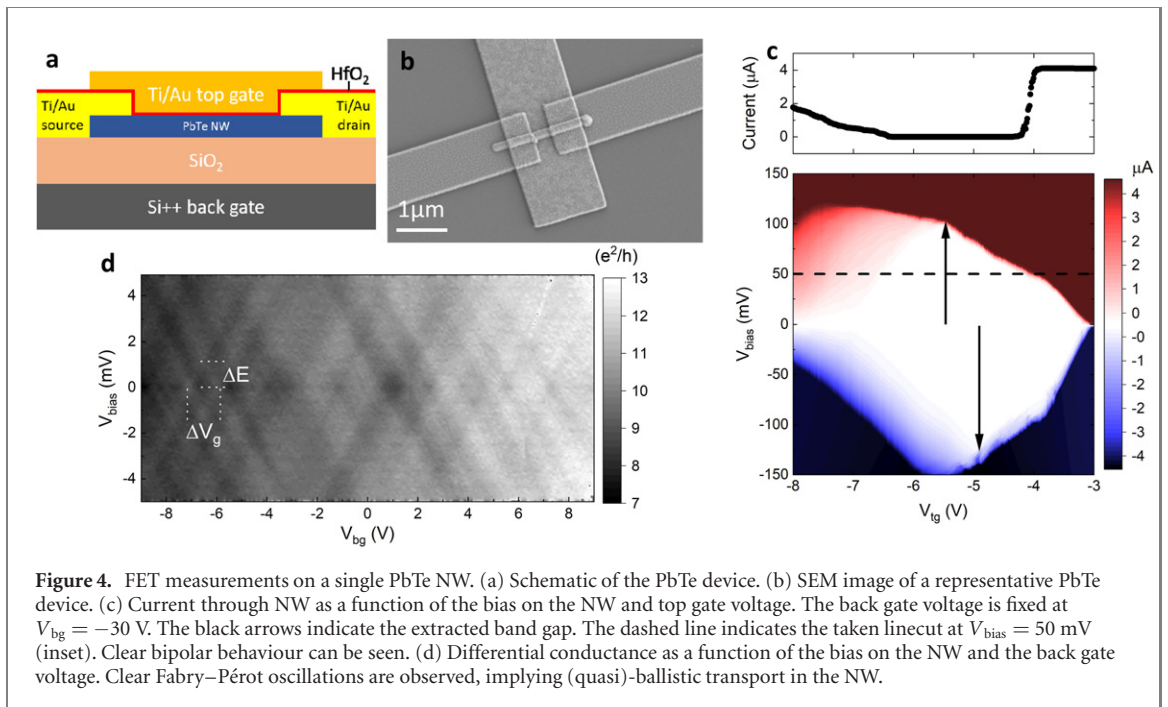
Next, we study the crystal structure and growth direction of the PbTe NWs by TEM, shown in figure 2. The analysis in figures 2(a)–(c) shows that the NWs grow in a [100] crystal direction. Figure 2(a) reveals a uniform diameter along the NW confirming the non-tapered growth. A thin (2 nm) self-terminating native oxide is present on the NW surface (figure 2(b)), leading to some roughening of the smooth side facets which could in the future be avoided by *in situ* passivation in the MBE system. HAADF-STEM and electron diffraction (ED) images acquired along a zone axis orthogonal to the NW axis (figures 2(b) and (c)) show that the NWs are monocrystalline and defect-free. An analysis along a complete NW (SI figures 3 and 4) confirms the monocrystalline structure. No pre- or post-growth segments with defects are found. The cross sectional TEM image in figure 2(d) illustrates that the wires have a square cross section, and are terminated by {200} facets, which are the lowest free-energy facets in PbTe [26]. EDX elemental analysis (figure 2(e)) shows that the NW indeed consists of both Pb and Te. The elemental mappings of the catalyst particle display a particle predominantly consisting of Pb, with Au present in the core. There are two likely mechanisms that can result in this separation: (1) during growth the Pb and Au are alloyed, after which segregation occurs during cooling down [27], or (2) the Au particle acts as a collection point for Pb at the start of the growth without alloying, allowing a droplet of Pb to form which then facilitates self-catalysed VLS growth. Except the catalyst particle on top the NW, no Au was detected to be incorporated in the NW above the detection limit of EDX (~ 1 atomic%).

The NW composition is further investigated using APT, which has a detection limit of around 1 ppm. An APT sample is prepared following the procedure discussed in the experimental section. An SEM image of a PbTe NW on a post is shown in figure 3(a). The top part, indicated by the yellow area, of this wire has been analysed by APT. A reconstruction of the NW is shown in figure 3(b), indicating a uniform distribution of the elements. The concentration of the detected elements is shown versus the axial position in figure 3(c). Besides Pb and Te, approximately 1 atomic% Se is detected, which is the result of contamination from the Se source in the MBE growth chamber. As Se has the same valency as Te, it will not affect the carrier density in the NWs, but it may have an effect on the carrier mobility due to alloy scattering. No other elements (Au from the catalyst droplet, In from the sample soldering, Ga and As from the growth substrate) are found in the PbTe NW above the detection limit.

In order to study the electronic properties single NW devices are fabricated, shown schematically in figure 4(a). Figure 4(b) shows an SEM image of a representative device with the distance between the contacts $d_{\text{cont}} \approx 300$ nm and a NW width $d_{\text{nw}} \approx 120$ nm. All measurements are done in a dilution refrigerator with a base temperature of 40 mK. All devices have Ohmic contacts, two representative I–V traces are shown in SI figure 5. The current through the NW is mapped using the source-drain bias V_{bias} and the top gate bias V_{tg} in figure 4(c). The back-gate voltage is kept constant at $V_{\text{bg}} = -30$ V. The extent of the non-conducting regime reflects the electrostatic doping of the NW within the PbTe band gap, which results in an estimated band gap of $E_{\text{g}} \sim 0.13 \pm 0.03$ eV at 50 mK, which is comparable to the expected value [28] of $E_{\text{g}} \sim 0.18$ eV at $T \sim 0$ K. The discrepancy may originate from below-gap tunnelling and disorder along the NW. From a linecut at $V_{\text{bias}} = 50$ mV the typical current as a function of the top-gate voltage is shown. At sufficiently high top-gate voltage ($V_{\text{tg}} > -4$ V), the Fermi level is tuned into the conduction band and current is mediated by electrons. When decreasing the top-gate voltage, a pinch off regime is present between $V_{\text{tg}} = -6.5$ V and $V_{\text{tg}} = -4$ V. When tuning the top-gate voltage even lower ($V_{\text{tg}} < -6.5$ V), the Fermi level is lowered into the valence band



and a hole conductance is measured. The hole current is significantly lower than the electron current, which can be due to a lower hole mobility or a smaller hole transparency at the NW-metal contact [29]. Electron and hole mobilities can, in principle, be estimated from the field effect and from the steepness of the pinch-off traces. The method has limitations, since it requires the unknown gate capacitance as an input, which is challenging to estimate given the ultrahigh dielectric constant of PbTe. A short discussion on the difficulties in estimating mobility is presented in SI section 5. We obtain indirect evidence of ballistic or quasiballistic transmission from the analysis of quantum oscillations of conductance. In another NW device, using the much weaker coupled back-gate instead of the strongly coupled top-gate, quasi-periodic oscillations are observed in the conductance for a wide range of V_{bg} (figure 4(d)). This is a manifestation of Fabry–Pérot type interference in the NW, arising from electrons reflecting either at the NW-metal contacts or between defects within the NW. Likely two or more oscillating modes are present, leading to the slowly changing background of the conductance [30]. Excessive disorder and scattering would lead to the loss of phase coherence and smearing of the Fabry–Pérot oscillations, while their presence can be used to estimate the mean free path and gate capacitance. The length L_c of the segment over which the Fabry–Pérot interference takes place can be approximated by [31] $L_c = \sqrt{\frac{\hbar^2 \pi^2}{2m^* \Delta E}}$, with $m^* = 0.02m_e$ the effective electron mass [32] and $\Delta E = 0.8\text{--}1.2$ meV the energy spacing of the Fabry–Pérot resonance. This results in $L_c = 125\text{--}150$ nm, which is approximately half of the NW channel and similar to the NW width. This result suggests that the transport in the NW is quasiballistic,



with a mean free path in the same length scale as the Fabry–Pérot cavity. Additional data from 3 other NW devices can be found in SI figure 6. Despite the mentioned uncertainties, this analysis shows that PbTe NWs are promising for quantum devices and should be investigated further as a host of one- and zero-dimensional states.

4. Conclusions and outlook

Single-crystalline, high aspect-ratio PbTe NWs are grown by the VLS mechanism in an MBE chamber using Au catalysts. The defect-free NWs grow in the [100] direction, with smooth {200} side facets, which are roughened by oxide formation after removal from the vacuum chamber. The Pb/Te ratio during growth determines the NW aspect ratio, and NWs with a length up to $3 \mu\text{m}$ are obtained without tapering. The increased length of the NWs allows for the fabrication of single NW FET devices, in which bipolar transport and Fabry–Pérot oscillations are observed at low temperature. This leads us to believe that electron transport in the device is at least quasiballistic, indicating the high quality of the grown material. Further studies should be directed towards the optimization of the PbTe NWs transport properties. As the oxidized surface likely leads to disorder, the NW surface should be passivated *in situ* after NW growth or prior to device fabrication. Possible passivation materials are lattice matched crystalline materials with a larger band gap such as CdTe and high-quality dielectrics such as Al_2O_3 or HfO_2 . Additionally, it will be interesting to explore the deposition of superconducting Pb *in situ* in order to achieve an epitaxial PbTe/Pb semiconductor-superconductor interface.

Acknowledgments

The authors thank Martijn Dijkstra, Marissa Roijen and Bart van der Looij for the support with the MBE reactor and Philipp Leubner and Maarten Kamphuis for helpful discussions. The work in Eindhoven is supported by the European Research Council (ERC TOCINA 834290), and Microsoft Corporation Station Q. We acknowledge Solliance, a solar energy R&D initiative of ECN, TNO, Holst, TU/e, imec and Forschungszentrum Jülich, and the Dutch province of Noord-Brabant for funding the TEM facility. Transport measurements in Pittsburgh are supported by NSF PIRE-1743717, NSF DMR-1906325, ONR and ARO. The APT work was supported by NSERC Canada (Discovery, SPG, and CRD Grants), Canada Research Chairs, Canada Foundation for Innovation, Mitacs, PRIMA Québec, and Defence Canada (Innovation for Defence Excellence and Security, IDEaS).

Conflict of interest

The authors declare no conflict of interest.

Data availability statement

The data that support the findings of this study are available upon reasonable request from the authors.

ORCID iDs


Sander G Schellingerhout  <https://orcid.org/0000-0002-7093-3362>

Xin Guan  <https://orcid.org/0000-0002-6395-8537>

Yifan Jiang  <https://orcid.org/0000-0001-6113-7666>

Max S M Hoskam  <https://orcid.org/0000-0003-4491-4536>

Jason Jung  <https://orcid.org/0000-0001-9865-9732>

Sebastian Koelling  <https://orcid.org/0000-0002-6606-9110>

Oussama Moutanabbir  <https://orcid.org/0000-0002-0721-3696>

Marcel A Verheijen  <https://orcid.org/0000-0002-8749-7755>

Sergey M Frolov  <https://orcid.org/0000-0001-9259-6056>

Erik P A M Bakkers  <https://orcid.org/0000-0002-8264-6862>

References

- [1] Nadj-Perge S, Frolov S M, Bakkers E P A M and Kouwenhoven L P 2010 Spin-orbit qubit in a semiconductor nanowire *Nature* **468** 1084–7
- [2] Lutchny R M, Bakkers E P A M, Kouwenhoven L P, Krogstrup P, Marcus C M and Oreg Y 2018 Majorana zero modes in superconductor-semiconductor heterostructures *Nat. Rev. Mater.* **3** 52–68
- [3] Mourik V, Zuo K, Frolov S M, Plissard S R, Bakkers E P A M and Kouwenhoven L P 2012 Signatures of Majorana fermions in hybrid superconductor-semiconductor nanowire devices *Science* **336** 1003–7
- [4] Pendharkar M et al 2021 Parity-preserving and magnetic field-resilient superconductivity in InSb nanowires with Sn shells *Science* **372** 508–11
- [5] Deng M T, Vaitiekėnas S, Hansen E B, Danon J, Leijnse M, Flensberg K, Nygård J, Krogstrup P and Marcus C M 2016 Majorana bound state in a coupled quantum-dot hybrid-nanowire system *Science* **354** 1557–62
- [6] Kringhøj A et al 2021 Magnetic-field-compatible superconducting transmon qubit *Phys. Rev. Appl.* **15** 054001
- [7] Froning F N M et al 2020 Ultrafast hole spin qubit with gate-tunable spin-orbit switch *Nat. Nanotechnol.* **16** 308–12
- [8] Springholz G 2013 Molecular beam epitaxy of IV–VI semiconductors *Molecular Beam Epitaxy* (Amsterdam: Elsevier) pp 263–310
- [9] Assaf B A, Phuphachong T, Volobuev V V, Inhofer A, Bauer G, Springholz G, de Vaulchier L A and Guldner Y 2016 Massive and massless Dirac fermions in $\text{Pb}_{1-x}\text{Sn}_x\text{Te}$ topological crystalline insulator probed by magneto-optical absorption *Sci. Rep.* **6** 20323
- [10] Liu P, Williams J R and Cha J J 2019 Topological nanomaterials *Nat. Rev. Mater.* **4** 479–96
- [11] Springholz G, Bauer G and Ihninger G 1993 MBE of high mobility PbTe films and $\text{PbTe}/\text{Pb}_{1-x}\text{Eu}_x\text{Te}$ heterostructures *J. Cryst. Growth* **127** 302–7
- [12] Yuan S, Krenn H, Springholz G, Ueta Y, Bauer G and McCann P J 1997 Magnetoreflexivity of $\text{Pb}_{1-x}\text{Eu}_x\text{Te}$ epilayers and $\text{PbTe}/\text{Pb}_{1-x}\text{Eu}_x\text{Te}$ multiple quantum wells *Phys. Rev. B* **55** 4607–19
- [13] Liu W, Cai W and Yao L 2007 Electrochemical deposition of well-ordered single-crystal PbTe nanowire arrays *Chem. Lett.* **36** 1362–3
- [14] Yang Y, Kung S C, Taggart D K, Xiang C, Yang F, Brown M A, Kruse T J, Hemminger J C and Penner R M 2008 Synthesis of PbTe nanowire arrays using lithographically patterned nanowire electrodeposition *Nano Lett.* **8** 2447–51
- [15] Tai G A, Zhou B and Guo W 2008 Structural characterization and thermoelectric transport properties of uniform single-crystalline lead telluride nanowires *J. Phys. Chem. C* **112** 11314–8
- [16] Fardy M, Hochbaum A I, Goldberger J, Zhang M M and Yang P 2007 Synthesis and thermoelectrical characterization of lead chalcogenide nanowires *Adv. Mater.* **19** 3047–51
- [17] Jang S Y, Kim H S, Park J, Jung M, Kim J, Lee S H, Roh J W and Lee W 2009 Transport properties of single-crystalline n-type semiconducting PbTe nanowires *Nanotechnology* **20** 415204
- [18] Roh J W, Jang S Y, Kang J, Lee S, Noh J-S, Kim W, Park J and Lee W 2010 Size-dependent thermal conductivity of individual single-crystalline PbTe nanowires *Appl. Phys. Lett.* **96** 103101
- [19] Lee S H, Shim W, Jang S Y, Roh J W, Kim P, Park J and Lee W 2011 Thermoelectric properties of individual single-crystalline PbTe nanowires grown by a vapor transport method *Nanotechnology* **22** 295707
- [20] Dziawa P et al 2010 Defect free PbTe nanowires grown by molecular beam epitaxy on GaAs(111)B substrates *Cryst. Growth Des.* **10** 109–13
- [21] Volobuev V V, Stetsenko A N, Mateychenko P V, Zubarev E N, Samburskaya T, Dziawa P, Reszka A, Story T and Sipatov A Y 2011 Bi catalyzed VLS growth of PbTe (001) nanowires *J. Cryst. Growth* **318** 1105–8
- [22] Koelling S, Li A, Cavalli A, Assali S, Car D, Gazibegovic S, Bakkers E P A M and Koenraad P M 2017 Atom-by-atom analysis of semiconductor nanowires with parts per million sensitivity *Nano Lett.* **17** 599–605
- [23] Fraser G W 2002 The ion detection efficiency of microchannel plates (MCPs) *Int. J. Mass Spectrom.* **215** 13–30
- [24] Costa G D, Wang H, Duguay S, Bostel A, Blavette D and Deconihout B 2012 Advance in multi-hit detection and quantization in atom probe tomography *Rev. Sci. Instrum.* **83** 123709
- [25] Mengui U A, Abramof E, Rappi P H O, Díaz B, Closs H, Senna J R and Ueta A Y 2009 Electrical properties of PbTe doped with BaF_2 *J. Appl. Phys.* **105** 043709
- [26] Egerton R F 1971 Surface free energies of lead telluride *Surf. Sci.* **24** 647–50
- [27] Evans D S and Prince A 1982 The Au–Pb phase diagram *MRS Proc.* **19** 383

- [28] Madelung O 2004 *Semiconductors: Data Handbook* (Berlin: Springer)
- [29] Pribiag V S, Nadj-Perge S, Frolov S M, van den Berg J W G, van Weperen I, Plissard S R, Bakkers E P A M and Kouwenhoven L P 2013 Electrical control of single hole spins in nanowire quantum dots *Nat. Nanotechnol.* **8** 170–4
- [30] Kretinin A V, Popovitz-Biro R, Mahalu D and Shtrikman H 2010 Multimode Fabry–Pérot conductance oscillations in suspended stacking-faults-free InAs nanowires *Nano Lett.* **10** 3439–45

- [31] Kotekar-Patil D, Nguyen B-M, Yoo J, Dayeh S A and Frolov S M 2017 Quasiballistic quantum transport through Ge/Si core/shell nanowires *Nanotechnology* **28** 385204
- [32] Grabecki G *et al* 2005 Disorder suppression and precise conductance quantization in constrictions of PbTe quantum wells *Phys. Rev. B* **72** 125332